Oil droplet formation and vertical transport in the upper ocean

Ruixue Liu[1], Michel C. Boufadel[1*], Lin Zhao[2], Tim Nedwed, Kenneth Lee[3], Guillaume Marcotte[4], Christopher Barker[5]

[1] *Center for Natural Resources, Civil and Environmental Engineering Department, New Jersey Institute of Technology, Newark, NJ 07102, USA*

[2] *ExxonMobil Upstream Research Company, Houston, TX 77389, USA*

[3] *Department of Fisheries and Oceans, Dartmouth, Canada*

[4] *Canadian Centre for Meteorological and Environmental Prediction, National Operation Division, Environmental Emergencies Section, Environment and Climate Change Canada, Dorval, QC, Canada*

[5] *Office of Response and Restoration, NOAA, Seattle, WA 98115, USA*

[*]Corresponding author: *Michel C. Boufadel (boufadel@gmail.com)*

1. Abstract

The dispersion of oil droplets following a surface oil spill is important for evaluating the impact to the environment. Under breaking wave conditions, the surface oil experiences mainly two processes: (1) the generation of oil droplets at/near the water surface and (2) the vertical transport of oil droplets due to ocean dynamics in the surface layer and the interior. We investigated this behavior by incorporating the vertical transport equation and the VDROP model (Zhao et al. 2014a). The transport equation adopted the ocean dynamics by K-profile parameterization (KPP) and the impact of additional turbulence by imposing the energy dissipation rate on the ocean surface. The breakup of oil droplets was accounted for by the VDROP model, which was based on the population dynamics for dispersed phase. The breakup and transport of oil was obtained in a 10 m mixed layer along with the evolution of time. The effect of oil slick thickness and the oil viscosity

were also investigated; and the discussion about the entrained droplet distribution and the entrainment rate were conducted. It was found out that the oil slick thickness only manipulates the quantity of oil in the water column, while the distribution and the transport tendency remain great similarity. On the other hand, the higher oil viscosity produces larger droplet sizes which also influence the transport of generated droplets. Moreover, although the entrained distribution and the entrainment rate shares certain consistency with previous study on entrainment models, divergences are also noticed in the current models. Accordingly, the model that describes the physics in the ocean turbulence conditions should be adopted in order to avoid incorrect qualification of the oil concentration dispersed in the ocean after oil spills.

2. Introduction

The increasing activities of offshore oil production and transport increased the probability of oil spills (NRC 2003). Oil on the water surface gets subjected to various elements in the environment including evaporation (Stiver and Mackay 1984, Lee et al. 2015), photooxidation (Garrett et al. 1998, Ward and Overton 2020), emulsification (Mackay and Zagorski 1982, Fingas et al. 1994), and dissolution (Gros et al. 2016, Gros et al. 2017). Also, oil slicks on the water surface could break into small droplets due to breaking waves, and because the buoyancy of droplets increases with the diameter, small oil droplets tend to migrate downward due to ocean turbulence. The process of droplet generation and subsequent transport of droplets in the water column is labelled as “oil dispersion” in the oil literature because it describes how oil droplets “disperse” in the water column. It is different from the traditional definition of dispersion that means spreading due to velocity gradients (Taylor 1953, Taylor 1954).The evolution and the

further transport of oil droplets in the water column is critical to assess the impact of oil spill on the ecosystem and communities (NRC 2003). The size of the oil droplet impacts their fate, as dissolution (Zhao et al. 2016, Stevens et al. 2017) and biodegradation(Prince et al. 2013, Socolofsky et al. 2019) increase with the droplet size, as these processes are interfacial-area dependent. Therefore, knowledge of the oil droplets size distribution (DSD) is important for determining the transport and fate of oil.

The current conceptual framework for the dispersion of oil in the water column relies on the work of Delvigne and Sweeney (G. A. L. Delvigne 1988), henceforth DS, who conducted breaking wave experiments in wave tanks of various scales and measured the oil DSD and the oil mass in the water column. They found that the number of droplets in the water column correlates with the diameter through the relation:

$$N(d) \propto d^{-2.3} \quad (1)$$

They also developed a formula to predict the entrained mass of oil in the water column based on wave properties and droplet size (discussed later in the manuscript). Numerous wave-tank studies of oil dispersion were conducted in wave tanks subsequently (Li et al. 2007, Li et al. 2008, Li et al. 2009a, Li et al. 2009b, Reed et al. 2009, Li et al. 2017a, Cui et al. 2020). Li et al. (2017a) and Cui et al. (2020) found that the DS correlation holds for diameters less than a millimeter, and the drop is rapid for larger diameters with an exponent of -9 in Eq. 1. Cui et al. (2020) explained the exponent of Eq. 1 and the "-9" exponent for larger diameters as due to a Gaussian volume-based DSD with a mean around a millimeter. Johansen et al. (2015) introduced equations that predict the volume based median diameter, d_{50}, based oil properties and wave hydrodynamics through the

usage of the dimensionless groups Reynolds and Weber. They also developed an expression for the entrainment of oil in the water column. Li et al. (2017) developed a similar approach.

The concept of "oil entrainment" into the water column due to breaking waves (Mackay et al. 1980, Mackay et al. 1986, Delvigne and Sweeney 1988a) has been the cornerstone of oil spill models of the 1990s, which is probably due to the fact that the focus then was on the transport of oil on the water surface, and to have a conceptual/numerical module to "get the oil out" of the water surface. However, such an approach does not "connect" the entrained mass of oil to the hydrodynamics in the water column beneath the waves. In addition, the entrainment expressions were developed in wavetanks, and thus do not account for the background turbulence present at sea. Furthermore, the most frequent wave breaking and/or whitecaps generation events at sea are due to wind shear rather than the focusing of waves as adopted in wavetanks. Therefore, breaking at sea does not penetrate too deep into the water column, and is typically less than 0.5 m (Vlahos and Monahan 2020). However, small air bubbles (tens of microns in diameter) from whitecaps have been measured down to 4 m and 10 m depths (Thorpe et al. 1992). Therefore, the transport of bubbles in the water column cannot be due to the breaking event, rather to turbulent diffusion.

Boufadel et al. (2020) investigated the transport of droplets up to 24 hours by adopting the K-profile parameterization eddy diffusivity model. They also provided a new dimensionless formulation to generalize the results and showed that the transport mainly

depends on water friction speed, the mixed layer depth and the droplet diameter. The above-mentioned model emphasized on the transport of oil droplets with various diameters with less discussion on the breakup of droplets.

We propose herein a new framework for addressing oil dispersion at sea that provides a means to incorporate small-scale (meter) processes into large-scale oil spill models. We consider that the role of whitecaps (or wave breakers) is to alter the oil droplet size distribution, and we consider that the vertical transport can be captured through an accurate formulation of the eddy diffusivity. We assume that droplet breakup occurs within a 10 cm layer, and we simulate the breakup using the droplet population model VDROP (Zhao et al. 2014b). We demonstrate our approach by assuming two oil slick thicknesses and two oil viscosities.

3. Methods

2.1 Ocean hydrodynamics

At the ocean surface, momentum from the wind transfers to the water through the shear stress and could manifest through wave breaking when the wind speed exceeds a few meters per second (Lehr and Simecek-Beatty 2000, Lehr et al. 2002). The turbulence level large within four to six wave heights (Drennan et al. 1992, Drennan et al. 1996, Terray et al. 1996). At the surface, the energy dissipation rate decreases rapidly with depth, as $z^{-2.4}$ (Craig and Banner 1994a). This region is labelled as the wave-enhanced layer. The wave enhanced layer is part of the mixed layer, where the law of the wall applies with correction due to the Coriolis force (Ekman 1905). The exact interpretation

of the depth of the mixed layer (MLD) is rather complicated in terms of temperature and density profile. The MLD depends on a variety of factors including wind speed, fetch, density and temperature gradients and the season. In large sea bodies, the MLD could be up to 120 m in winter and is usually less than 30 m in summer (Kara et al. 2000, de Boyer Montégut et al. 2004).

However, as the intrusion depth of oil droplets is generally within meters below the surface when it reaches equilibrium state, the depth of the mixed layer is defined as 10 m for rather calm ocean and mind wind speed herein. Beneath the mixed layer, the hydrodynamics tend to be independent of the local atmospheric forcing and to depend on the internal ocean waves, shear generation at the bottom, and buoyancy fluxes (due to salinity or temperature gradients). The ocean structure is illustrated in Fig. 1.

Wind exerts a tangential stress on the water surface that results in the generation of breaking waves and the transport of momentum in the water column (Okuda et al. 1977). It is common to assume a log layer for the horizontal velocity profile in air as:

$$U(h) = \frac{u_{a*}}{\kappa} Ln \frac{h}{z_o} + B.u_{a*} \qquad (2)$$

Where u_{a*} is the friction velocity in air, κ is the von Karman constant (0.4), and z_o is the roughness height, which can be estimated based on Charnok's law (Charnock 1955, Kitaigorodskii et al. 1983).

$$z_o = \frac{a.u_{a*}^2}{g} \qquad (3)$$

With a=12.5. Therefore, combining Eqs. 2 and 3, one may write:

$$h\exp\left(-\frac{\kappa U(h)}{u_{a*}}\right)=\exp(-a\kappa)\frac{u_{a*}^2}{g} \tag{4}$$

Typically, the wind speed is measured at h=10 m and thus the only unknown is the friction velocity u_{a*}. The transfer of shear to the water column occurs by equating the shear stress on both sides of the water-air interface:

$$u_*^2=\frac{\rho_{air}}{\rho_{water}}u_{a*}^2 \tag{5}$$

Where ρ_{air} and ρ_{air} are the density of air and water, respectively, and u_* is the friction velocity in water. Thus, the friction velocity in water is around 2 orders of magnitude smaller than its counterpart in air.

Knowledge of the water friction velocity allows one to estimate the energy dissipation rate and the eddy diffusivity in the water column. The profile of the energy dissipation rate is (Craig and Banner 1994b):

$\varepsilon \propto z^{-2.4}$ in the wave-enhanced layer (6a)

$\varepsilon \propto z^{-1}$ below the wave-enhanced layer (6b)

That is, the energy dissipation rate decreases sharply in the "wave-enhanced" layer (Figure 1) due to wave breaking. These arguments were produced in earlier works (Kitaigorodskii et al. 1983) and observed in field studies (Terray et al. 1996). The depth of the wave-enhanced layer is typically 4 to 6 wave heights.

The breakup of oil volumes into smaller droplets strongly depends on the energy dissipation rate (Zhao et al. 2014a), please see Eq. 12. And because of the rapid decrease of ε with depth in the wave-enhanced layer, it is reasonable for modeling purposes, to consider that ε takes a constant value in the upper part of the wave-enhanced layer and to be zero elsewhere. The value of ε to consider within $z_0 = 0.1\,\mathrm{m}$ is also important, as Eqs. 6 represent time-average behavior. However, within a time series, it is the large value of ε that cause the breakup (Baldyga and Podgórska 1998, Cui et al. 2020). Therefore, we will adopt herein an arbitrary value for the energy dissipation rate in the roughness height zo, and we will take $\varepsilon = 0.1$ watt/kg. This value is comparable to the energy dissipation rate reported in wave tanks (0.4 watt/kg in Cui et al, and 0.01 watt/kg in Li and Katz et al. 2017). It is also smaller but comparable to the energy dissipation rate in the EPA baffled flask at 200 rpm used for oil dispersion (0.7 watt/kg).

When the oil droplets are formed, they get transported in the water column due to their own terminal rise velocity and due to turbulent diffusion. Thus, the variation of the

concentration of droplets of size "d" with time and space is modeled using the advection-diffusion equation:

$$\frac{\partial c_d}{\partial t} = \frac{\partial}{\partial z}\left(K \frac{\partial c_d}{\partial z} \right) - \frac{\partial}{\partial z}\left(w_d . c_d \right) + S \qquad (7)$$

where K is the eddy diffusivity, and w_d corresponds to the buoyancy velocity of droplets with various size d. And *S* is a source term representing the concentration variation with time (S is non zero only within the depth z_b).

The research on the eddy diffusivity K could be generally divided into two approaches: the bulk mixed-layer models and the differential mixed-layer models. The bulk model assumes the velocity, temperature and salinity are uniform in the MLD, and those physical quantities are discontinuous at the interface of the boundary and the deeper layer. Besides, the model also assumes that there is no velocity shear at the top layer, which disagrees with many experimental observations (Pollard and Millard Jr 1970, Halpern 1976).

The differential mixed-layer model employs the mixing length argument (Prandtl 1953) and a closure form for turbulence, and we believe it can better describe the physical quantities in the vertical direction. Previous models include KPP (Large et al. 1994), MY (Mellor and Yamada 1982) and CD (Canuto and Dubovikov 1996). Among them, the K-

profile parameterization (KPP) model is one of the most commonly used models, in which the flux of material F due to turbulent diffusion is given by:

$$F = -K(\frac{\partial c}{\partial z} - \gamma) \tag{8}$$

where c is any passive scalar such as number concentration, γ is a gain parameter which represents a convective flux superimposed on the diffusive flux and introduces the non-local characteristic. Derived from the KPP model, the research domain herein is focused on the one-dimensional vertical transport, where the eddy diffusivity could be further simplified to a third-order polynominal as a function of water depth (Large et al. 1994, Boufadel et al. 2020). We also make an effort herein to account for the surface roughness z_0 by altering the original (or standard) expression of the KPP model, viz:

$$K = \frac{\kappa u_*}{\phi}(z + z_0)(1 - \frac{z}{\mathrm{MLD}})^2 \tag{9}$$

where the constant $\phi = 0.9$.

The droplet rising velocity (terminal) velocity due to buoyancy for a droplet of diameter "d" is given by:

$$w_d = -\sqrt{\frac{4gd(\rho_w - \rho_o)}{3C_D\rho_w}} \tag{10a}$$

where ρ is the density $(\mathrm{kg/m^3})$; the subscript of o and w indicates the properties of oil and water, respectively; the negative sign indicates that the buoyancy is opposite to the

coordinate direction, where the positive direction is pointing downwards. C_D is the coefficient of drag, given by Naumann and Schiller (1935):

$$C_D = \begin{cases} \dfrac{24(1+0.15\,\mathrm{Re}_d^{0.687})}{\mathrm{Re}_d} & \mathrm{Re}_d \le 1000 \\ 0.44 & \mathrm{Re}_d > 1000 \end{cases} \qquad (10b)$$

The term $\mathrm{Re}_d = \dfrac{\rho_w w_d d}{\mu_w}$ is the droplet rise velocity Reynolds number, characterizing the hydrodynamics around the droplet, and it should not be confused with the Reynolds number of the large-scale hydrodynamics; μ_w is the dynamic viscosity $(\mathrm{Pa}\cdot\mathrm{s})$ of water. Substituting Eq. 10(b) into Eq. 10(a) gives the profile of the rising velocity as a function of droplet diameter as shown in Fig. 3(a).

2.2 Oil droplet formation within the depth z_0, the VDROP model

The term S in Eq. 7 represents the formation of oil droplets in the water column, a process governed by a balance between destructive forces due to the hydrodynamics and resisting forces due to the oil-water interfacial area and oil viscosity. The population balanced model describes the evolution of droplets accounting for the breakup due to destructive forces and the coalescence due to resisting forces, meanwhile maintaining the mass balance. Based on this theory, Zhao et al. (2014a) developed a numerical model VDROP to simulate the transient and steady-state oil droplet size distribution. The main concept could be summarized as:

$$\frac{\partial n(d_i,t)}{\partial t} = \sum_{j=i+1}^{n} \beta(d_i,d_j) g(d_j) n(d_j,t) - g(d_i) n(d_i,t) + \underbrace{\sum_{j=1}^{n}\sum_{k=1}^{n}}_{v_j+v_k=v_i} \Gamma(d_j,d_k) n(d_j,t) n(d_k,t) - n(d_i,t) \sum_{j=1}^{n} \Gamma(d_i,d_j) n(d_j,t) \tag{11}$$

where $n(d_i,t)$ is the number concentration of droplets of diameter d_i at given time t; $\beta(d_i,d_j)$ is the breakage probability density function, $\Gamma(d_i,d_j)$ is the coalescence rate and $g(d)$ is the breakage rate function, computed as:

$$g\left(d_i\right) = K_b \int_{n_e} S_{ed} \left(5.15 * (\varepsilon d_e)^{2/3} + 1.06 * (\varepsilon d_i)^{2/3}\right)^{1/2} BE\left(d_i, d_e, \varepsilon, t\right) \mathrm{d}n_e \tag{12}$$

where the term $S_{ed} = \pi / 4(d_e + d_i)^2$ is the collision cross-section area of eddy whose diameter is d_e and a droplet with a diameter of d_i; n_e is the number concentration of eddies; K_b is a system-dependent parameter; $BE\left(d_i, d_e, \varepsilon, t\right)$ is the breakage efficiency term, which is calculated as:

$$BE\left(d_i, d_e, \varepsilon, t\right) = \exp\left[-\frac{1}{c_1}\left(\frac{E_c + E_v}{e}\right)\right] \tag{14}$$

where c_1 is an empirical constant equal to 1.3; E_c is the average excess of surface energy needed to form a pair of daughter droplets or a small and large droplets, this term also known as formation energy; E_v is the resistance energy due to viscous force within the

droplet, e is the energy of the turbulent eddy that would cause the breakup of the droplet; the expressions of these terms are found in Zhao et al. (2014a).

In Zhao et al. (2014a), the breakage rate $g(d_i)$ is integrated from the smallest eddy size to the desired droplet size, which ranged from micron to millimeter. The computation of integration is rather time consuming when computing the breakage rate $g(d_i)$. Yet in our case, the energy dissipation rate ε was considered constant and uniform within the depth z_b, accordingly, the only variables for breakage rate is the droplet diameter. This allows the constant relation between the breakage rate and the droplet diameter, which requires only one time calculation before running the VDROP module. In this way, the computation efficiency was substantially increased with no loss of accuracy compared to the original equation.

2.3 Initial and boundary conditions

To model the transport and breakup of the oil on the surface, the initial and boundary conditions are discussed here. The initial conditions are:

$$c_d(z, t=0) = \begin{cases} c_{d,ini} & 0 \le z \le z_{ini} \\ 0 & z > z_{ini} \end{cases} \quad (15)$$

where z_{ini} is the initial releasing depth of the oil (adopting 0.01 m here).

The initial droplet size d_{ini} and the initial concentration $c_{d,ini}$ need to be properly modelled. It is assumed that the initial droplet volume is equal to the cylinder whose radium is the Taylor microscale of turbulence λ, and the height of the oil slick thickness h, shown as Fig. 3(b):

$$V = \pi\lambda^2.h \tag{16}$$

The height h is usually assumed to between 0.1~2 mm and the Taylor microscale λ can be estimated based on the Kolmogorov length scale (Tennekes 1972, Pope 2000):

$$\lambda=\sqrt{10}\eta^{2/3}l^{1/3} \tag{17}$$

where l is the length scale of larger eddies, and could be taken equal to the roughness height of the water surface z_0, and η is the Kolmogorov microscale given by:

$$\eta=\left(\frac{\nu^3}{\varepsilon}\right)^{\frac{1}{4}} \tag{18}$$

Assuming the volume of oil converts into a sphere, the diameter of that sphere is given by:

$$d_{ini}=\left(\frac{6V}{\pi}\right)^{1/3}=\left(\frac{6}{\pi}\frac{\pi}{4}\lambda^2.h\right)^{1/3} \tag{19}$$

Similarly, it was assumed that the initial droplet volume only contained the largest droplet d_{ini} and uniformly distributed in the simulation grid within the initial releasing

height z_{ini}. Because of one-dimensional simulation, the length and width of the simulation domain was assumed to be unit $1\,m \times 1\,m$. Accordingly, the initial volume concentration is given by:

$$V(z,t=0)=\begin{cases}\dfrac{h}{z_{ini}} & z \le z_{ini} \\ 0 & z > z_{ini}\end{cases} \tag{20}$$

And the initial number concentration is given by:

$$c_d(z,t=0)=\begin{cases}\dfrac{1}{\dfrac{\pi}{6}d_{ini}^3}\dfrac{h}{z_{ini}} & 0 < z < z_{ini} \\ 0 & z > z_{ini}\end{cases} \tag{21}$$

The boundary conditions are:

$$-K\frac{\partial c_d}{\partial z}+w_d.c_d(z=0,t)=0 \tag{22 a}$$

$$\frac{\partial c_d(z=\infty,t)}{\partial z}=0 \tag{22 b}$$

The Eq. 22 (a) denotes that at the water surface ($z=0$), the total flux of oil is equal to zero (i.e. the oil does not cross the water surface); and at infinite depth (i.e. at a large distance from the surface, here adopted twice of MLD), it is assumed that the gradient of concentration is zero, which means that droplets leave the bottom by advection but not diffusion. When eddy diffusivity is uniform through the water and no breakup event happens, the analytical solution could be found in Van Genuchten (1982) and Boufadel et al. (2020).

2.4 Numerical coupling between transport and droplet formation

The calculation of the submerged oil droplets behavior needs the overall description of ocean hydrodynamics, the transport process and the formation process as previously discussed. Accordingly, an integral model coupling of these implementations is introduced here and the schematic of the coupling process is illustrated in Fig. 4. Generally, a number of droplets of a given (large) size are released at time t=0 s and within a depth z_{ini}; those droplets are then going through the breakup process (VDROP), which allows the break of large droplets and the generating of small droplets. Upon the finish of droplet evolution, the updated droplets are used to compute the transport process, which allows the vertical migration of droplets in the water column due to buoyancy and turbulent diffusion. The concentration and location of droplets are then updated and go through the next iteration.

Numerically, the oil droplets are assigned into different size bins, for every iteration process Δt, the VDROP is first applied to all size bins located in one cell Δz repeatedly, obtaining the updated oil concentration for each cell. Based on the new concentration, the transport equations are computed to all cells for each size bin d_i repeatedly, resulting in the final updated oil concentration for one iteration. The process repeats until the end of simulation. In particular, the time interval of the breakup (VDROP) process was assumed to be Δt_1 while the transport process was assumed to be repeated with a time interval Δt_2.

For accuracy considerations, particularly for droplets within millimeter scale, the time interval Δt_1 of VDROP is normally chosen to be very small (Zhao et al. 2014a), which is adopted as 0.001 s in current investigation. On the other hand, the implicit method with center-difference for the second order gradient was employed for transport equation. Because the implicit method of solving the transport equation offers rather good stability, the time interval Δt_2 could be endowed with comparably large value compared with Δt_1 to avoid imposing unreasonable computational demands. Adjusted to the total simulation time, Δt_2 was set to be 0.01 s. Although the two processes were computed in sequence, it was assumed the two processes occurred simultaneously, which is more analogous to the reality where the droplets are breaking while being transported within the water column. Accordingly, one iteration of droplet evolution is formed by one Δt_2 and N Δt_1 where the number of N satisfied $N\Delta t_1 = \Delta t_2 = \Delta t$.

The discretization of the ocean domain was divided into two groups: near the boundary section and section between the top and bottom boundary. The depth interval Δz near boundary ($0 \le z \le 2$ m) is set as fine as 1×10^{-3} m. Also, in order to satisfy the bottom boundary condition where the concentration gradient is zero at the infinity, the simulation domain was extended into 20 m (twice of the MLD). And near the bottom boundary $18 \le z \le 20$ m, the fine Δz (1 mm) was also adopted. Between the two near-boundary sections, the droplets are sparse and therefore a coarse grid $\Delta z = 0.1$ m was employed to

save computation resources. The other general simulation setup including the oil and water properties, together with the previous demonstration, are listed in Table 1.

A typical case was specified at dynamic oil viscosity of 22.2 cP and oil slick thickness of 0.1 mm. According to Eq. 16~19, the initial droplet size is 4.11 mm, taken for 4 mm here with the 50 μm size bin increment, which results in a total of 80 size bins. Consequently, the initial number concentration c_{ini} is 2.98×10^5 #/m^3 based on Eq. 21. Additionally, distinct spill incidence leads to varied spilled amount and spreading area, which results in different oil slick thickness; thus, apart from the 0.1 mm thickness, we chose the other thickness of 1 mm to investigate its behavior. Another coefficient that may affect the dispersion of oil droplet is the oil viscosity. The addressing of oil viscosity is of importance as the oil will endure the weathering process on the ocean surface. Therefore, a case with 88.7 cP oil viscosity was also evaluated here, leaving a total of four cases. Note that the varied oil slick thickness and oil viscosity will lead to different initial droplet size and initial number concentration; the number of size bins will also change under the same size bin interval of 50 μm. The detailed quantities for the four cases are listed in Table 2, while other simulation setup are identical as Table 1.

4. Results

For subsequent outcome, the oil droplet size distribution is reported as volume distribution instead of number distribution as such has a more environmental implication. The number concentration ($\#/m^3$) was converted into volume concentration (m^3/m^3) by multiplying

the droplet volume for each bin. Meanwhile, the volume concentration was equivalent to the mass of droplets after multiplying the grid volume ($\Delta z \times 1 \times 1\ \mathrm{m}^3$) and the density of the oil, which were uniform for all kinds of droplets.

For the first case, the volume concentration as a function of depth z is shown in Fig. 5 for droplets at time of 2, 4, 6, 8 s. One horizontal bar indicates the droplets concentration in one cell (Δz), while each colored grid indicates different size bins (droplet diameters). Although the largest bin is up to 4 mm, those large droplets rapidly broke down to small droplets and therefore only droplets up to 1 mm are shown here. Also, the cells are shown with intervals of four for concise expression. Generally, by comparing the four pots, the larger droplets (closer to yellow color) were disappearing along with increasing time and the volume concentration for smaller droplets (closer to blue color) were increasing. This indicates that the droplets are breaking into smaller droplets under the turbulence condition in the ocean surface. Meanwhile, along with the increment of time, more droplets were diffused into deeper water. For example, at t=2 s, there was barely existing of droplet at $z = 0.08\ \mathrm{m}$ cell, but a noticeable amount of them showed up at t=8 s. Apart from the variation with time, by examining the distribution of size bins at each cell, it could be deduced that the majority of the volume was occupied at the middle region (d=0.4~0.55 mm) after a longer time, while the smaller droplets and larger droplets took significant less portion. An appropriate approach to describe the droplet distribution is by the Gaussian distribution, which will be investigated in the later discussion section.

A more compact way to identify the droplet distribution is the d_{50} as shown in Fig. 6. The volume median diameter d_{50} is defined as the median for a volume distribution (the cumulative volume fraction equals to 50%), which reveals the characteristic droplet sizes within the one cell of depth z, namely, the higher d_{50} indicates a larger species of droplets group. From Fig. 6, at various time step, the d_{50} generally decreased along with the increasing depth, indicating a greater portion of smaller droplets immersed in the deeper layer, leaving larger droplets at the shallower locations. At t=8 s, the d_{50} ranges from 0.4 to 0.55 mm, which is in accordance with our previous discussion about droplet size distribution. Similarly, along with the increase of time, the overall trend of d_{50} was horizontally moving to the left-hand side, which suggests a notably declining of general droplet sizes due to the continuous breakup of large droplets. This is also verified by our previous observation, but moreover, as the gap between the two time steps becomes narrower with time, for instance, the differences between the second and fourth seconds are obviously larger than the differences between sixth and eight seconds. It implies that the breaking event tends to be stabilized after the diminishing of larger droplets.

For the purpose of assessing the transport behavior of droplets with varied diameters, we assumed the intrusion depth so that the cumulative mass along with the depth reaches 99% of the total current mass for each size bin. By this definition, the volume concentration (solid lines) and the intrusion depth (dashed lines) are shown in Fig. 7 for Case 1 at t=8 s. The various colored lines indicate droplet diameters of 0.05 mm, 0.2 mm, 0.4 mm and 0.6 mm, respectively. The plot demonstrated that, the smallest droplets (0.05 mm) had a largest intrusion depth (~0.19 m) while the droplets with a diameter of 0.6 mm

only reached 0.12 m. This is consistent with experimental observations where the small droplets have a faster downward flux and tend to penetrate deeper while the large droplet tend to float at shallow locations due to greater buoyancy.

After the demonstration of the results for the typical case with oil slick thickness h=0.1 mm and oil viscosity of 22.2 cP (Case 1 in the Table 2), the results for the other three cases were also analyzed correspondingly. The overall volume concentration for different cases at t=8 s is shown in Fig. 8. The first two cases (the two plots in the first row) had the same oil properties but the oil slick thickness h was adjusted to 0.1 mm and 1 mm, respectively. As stated earlier in the method sections, the variation of oil slick thickness would differ the initial amount of oil and the initial droplet size d_{ini}. Nevertheless, the tendency of the volume concentration was very similar to each other except for the amount of oil increased by one magnitude. This phenomenon was also identified between Case 3 and Case 4, which both share oil viscosity of 88.7 cP, but have different oil slick thickness of 0.1 mm and 1 mm. Consequently, it is reasonable to conclude that the initial droplet sizes have very limited effect on the distribution and transport of oil droplets; on the other hand, the dispersed amount of oil is proportional to the initial released oil amount on the surface, which is directly related to the oil slick thickness and the spreading area.

Also as illustrated by Fig. 8, the comparison between oil with different viscosity can be obtained by Case 1 versus Case 3 (the two plots on the left column) and Case 2 versus Case 4 (the two plots on the right column). It is obvious that the more large droplets

survived from breakup for higher viscosity oil cases, indicated by the appearance of yellow colored size bins. This suggests the effect of oil viscosity with respect to the resistance from breakup by turbulent eddies and facilitates the prediction of oil droplets when the oil viscosity increases during the spilling.

The result is also illustrated by the distribution of d_{50} as shown in Fig. 9. The d_{50} as a function of depth z for Case 1 and Case 2 is listed in the left-hand side, while the right-hand side represents the results for Case 3 and Case 4. The different color indicates the varied time at 2, 4, 6 and 8 s. Coinciding with previous observation, the distribution for the same viscosity cases exhibited great resemblance except that a little deviation was discriminated at an early stage of t=2 s for Case 3 and Case 4. This is predictable as the larger initial droplets require longer time to breakup but the discrepancy is eliminated shortly. Specifically, the d_{50} was 789 μm for Case 1 and Case 2 at t=2 near the surface; and it was gradually decreased to 532 μm at t=8 s. Besides, at deeper water z=0.1 m, the d_{50} decreased to 490 μm at t=2 s and 405 μm at t=8 s. Comparatively, the d_{50} was around 1000 μm for Case 3 and Case 4 at t=2 near the surface; and it was gradually decreased to 651 μm at t=8 s; at deeper water z=0.1 m, the d_{50} decreased to 540 μm at t=2 s and 443 μm at t=8 s. Generally, the high viscosity cases (Case 3 and Case 4) have larger droplet size everywhere in the water column than the low viscosity case (Case 1 and Case 2), yet, the divergence was scaled down in the deeper water column. The reason accounts for this is, although the high viscosity oil produces large droplets, only the droplets with equivalent sizes could be transported into deeper layers, leaving the large droplets in the upper section and therefore results in a more significant difference in the d_{50}.

5. Discussion

To compared with the previous entrainment models (Mackay et al. 1978, Delvigne and Sweeney 1988b, Tkalich and Chan 2002, French-McCay 2004, Reed et al. 2009), here we examined the droplets distribution that below z_{ini}, which serves a criterion for droplets being entrained in the water column. The results are shown in Fig. 10 for Case 1, where the mass of all the droplets of one size below z_{ini} were summed up. Generally, the entrained mass displays distributions that are analogous to the Gaussian curve. At t=2 s, the profile shows a slightly escalation of the right part, indicating a relatively under estimation of the larger droplets; nevertheless, along with the time, the profile of entrained mass matches the Gaussian distribution well and all four distributions remains good fittings with the coefficient of determination $R^2 \geq 95\%$.

As mentioned earlier, the DS relation predict the droplet size distribution following a wave breakup of the form $N(d) \sim d^{-2.3}$. This relation is equivalent to the volume/ mass of the droplet is linear related to the $d^{0.7}$, which means that the entrained mass is monotonically increased with diameter and is disagreed with our prediction. Nevertheless, while the logarithm of the Gaussian curve results in $-(d-\mu)^2$, for small values of d/μ ($d < \mu$), the mass distribution of droplets behaves as $-\mu^2 + 2\mu d$, which

is linearly dependent on the diameter d. The entrained mass computed at t=8 for Case 1 is fitted to droplet diameter and is shown in Fig. 11. The tendency shows a relation of $\sim d^{1.4}$, which is close to previous argument of linear dependence. But for the larger value of d/μ, the Gaussian curve indicates a decreasing tendency with d, i.e. the slope of the logarithm plot turns into negative. The possible reason could be justified that, along with the breakup of larger droplets, the total number or mass of the large droplets decreased rapidly as a function of droplet diameter. For example, Li et al. (2017a) concluded a correlation of $N \sim d^{-9.7}$, which was also verified by Cui et al. (2020).

Apart from the droplet distribution in the water, the concept of entrainment rate has been investigated. Delvigne and Sweeney (1988b) defined an empirical coefficient, the oil entrainment rate Q_r (kg/m^{2}s) as the dispersed oil mass in the water column per unit surface area per breaking event. They also characterized the oil entrainment by the dissipated energy of breaking waves, oil viscosity, oil layer thickness, temperature and decided the rate of entrainment Q_r by:

$$Q_r(d_o) = C^* D_{ba}^{0.57} d_o^{0.7} \Delta d \qquad (23)$$

where $Q_r(d_o)$ is the entrained mass of oil droplets with droplet sizes in an interval Δd around d_o (the interval $d_o - \frac{1}{2}\Delta d$ to $d_o + \frac{1}{2}\Delta d$); C^* is proportionality constant; D_{ba} is

dissipated breaking wave energy per unit surface area; C^* is varied for different types of crude oil. Li et al. (2017b) fitted C^* according to experimental data reported in Delvigne and Hulsen (1994):

$$C^* = \begin{cases} \exp\left(-0.1023\ln(\nu)+7.572\right) & \text{if } \nu < 132 \text{ cSt} \\ \exp\left(-1.8927\ln(\nu)+16.313\right) & \text{if } \nu > 132 \text{ cSt} \end{cases} \quad (24)$$

where ν is the kinematic viscosity of oil (cSt). Accordingly, for our targeted oil with viscosity of 22.2 cSt, C^* is adopted as 1400. For a typical large flume, D_{ba} takes value of 600 J/m^2; the entrainment rate Q_r as function of droplet diameter is shown in Fig. 12. The breaking wave energy per unit surface area D_{ba} (J/m^2) was derived from wave statistics; and in their experiment, D_{ba} (J/m^2) was found by subtracting the time-integrated energy fluxes before and beyond the breaker zone. Comparably, in our model, the energy dissipation rate ε (watt/kg) is employed instead of D_{ba}. Meanwhile, they could be converted by

$$D_{ba} = \varepsilon \frac{m_{cell} \cdot t}{A} \quad (25)$$

where A is the simulation area, which is 1×1 m^2 herein; and m_{cell} is the mass of roughness heights $m_{cell} = \rho_{water} V_{cell} = \rho_{water} z_0$; t is the simulation time. They argued that the minimum and maximum droplet diameter entrained in the water column were

assumed to be $0.1d_{50}$ and d_{50}, while droplets larger than d_{50} were found to resurface in less than one calculation time step so were not quantified as separate from surface slicks.

The entrainment rate was developed in wave tanks and heavily dependent on the wave characteristic. Yet, they do not account for the background turbulence that is present at sea, which leads to continuously breaking events. The actual ocean dynamics is also much more complicated than single wave events in wave tanks and therefore bringing difficulties in deciding the wave characteristic. Perhaps a more holistic approach would be to account for the role of the waves in producing oil droplets and to consider the transport to occur through the vertical eddy diffusivity, which can be obtained from experiments or hydrodynamic models. Therefore, here we obtained the entrainment rate Q_r by the integral model introduced in the method section as shown in Fig. 13.

The entrainment rate Q_r (kg/m^{2}s) obtained by our model was defined as the increment of the entrained droplet mass in every time step and was then divided the time step. For example, the entrainment rate at t=2 s was the entrained droplet mass at t=2 s subtracts the mass at t=1.99 s and divided by the time step ($\Delta t_2 = 0.01\,\mathrm{s}$). Generally, the profile of the entrainment rate shows a tendency close to a sine wave. Specifically, for small droplets, the entrainment rate increased with droplet diameters, which is in agreement with Delvigne and Sweeney (1988b). However, along with the increase of droplet diameters, the entrainment rate dropped down to a negative value. After the entrainment rate reached the minimum, the value was gradually back to zero. Moreover, by

comparing the four plots which represented entrainment rate at various time steps, the overall trend of entrainment rate was decreasing and the effective diameter range that the entrainment rate resumed to zero became narrower along with time. Delvigne and Sweeney (1988b) adopted d_{50} as the maximum entrained droplet diameter and Li et al. (2017b) also defined a maximum cutoff size for entrainment. For the results herein as Fig. 13, the sizes of droplet that cross the abscissa (i.e. $Q_r = 0$) could be correspondingly regarded as the maximum entrained droplet size. The droplets that were larger than the maximum entrained diameter and were breaking or/and resurfacing to the surface, resulting in a negative value of entrainment rate. Also, it could be detected from the plots that the values of the maximum entrained droplet diameter were decreasing with time, which was also suggested in Li et al. (2017b).

To conclude, the analysis from the results based on the current model conveys two messages. One of them is that the entrained mass/ volume distribution was firstly exponentially increased with the droplet diameter but then exponentially decreased with it. Instead of monotonically increasing with $d^{0.7}$, the Gaussian distribution is preferable to characterize the behavior, which was advised by Cui et al. (2020) and Boufadel et al. (2021) and is confirmed here. The other one is that, although the entrainment rate shared certain common features with the previous empirical equations, the description of it was rather complicated and contained time dependent parameters.

When droplets rise and reach the surface, they could spread into a thin slick, and it is possible that they would return to the water column smaller than they were. However, this also depends on the volume of oil at the water surface. Nevertheless, it is likely that our approach underestimates the number of small droplets in the water column.

6. Conclusion

A model incorporating transport behavior with breakup behavior (VDROP) for predicting oil droplets behaviors formed from surface oil spill was developed. The model quantifies ocean dynamics by adopting the K-profile parameterization (KPP) for eddy diffusivity and by imposing the energy dissipation rate on the ocean surface. Meanwhile, the breakup of oil droplets happens simultaneously at the upper layer, which is quantified by the population balanced equation model – the VDROP. The investigation demonstrated the oil droplet concentration, the d_{50} and the intrusion depth for a typical case. The results showed that under the turbulence conditions, the droplets continuously broke into smaller droplets; the smaller oil droplets were entrained deeper by the eddy diffusivity while the larger droplets aggregated more near the surface due to buoyancy. Similar analysis was conducted for cases with varied oil slick thickness and oil viscosity. The comparison among the four cases revealed that the oil slick thickness only altered the magnitude of the oil amount in the water column, while the distribution and the transport tendency remained great similarity. Besides, the increase of oil viscosity produced larger droplet sizes which then influenced the transport of generated droplets. Investigations about the entrainment droplet distributions and the entrainment rate were conducted and discussed. The entrained mass/volume distribution was exponentially increased with the droplet

diameter for small droplets but then exponentially decreased with it. Instead of monotonically increasing with $d^{0.7}$ as stated in Delvigne and Sweeney (1988b), the Gaussian distribution was preferable to characterize the behavior. For the entrainment rate, an increase with droplet diameter and a cutoff diameter were identified in current studies, which was also proposed in earlier research; however, the monotonically increasing was not sufficient to describe the overall tendency. Accordingly, we argued that the constant entrainment coefficient is not necessarily the desirable approach to predict the oil dispersed into the water. The description of the general ocean dynamics instead of a solitary breaking event should be considered, and the model that describes the breakup and transport physics should be adopted to adequately quantify the oil concentration dispersed in the ocean.

7. Reference

Baldyga, J. and W. Podgórska (1998). "Drop Break-up in Intermittent Turbulence: Maximum Stable and Transient Sizes of drops." The Canadian Journal of Chemical Engineering **76**: 456-470.

Boufadel, M., R. Liu, L. Zhao, Y. Lu, T. Özgökmen, T. Nedwed and K. Lee (2020). "Transport of oil droplets in the upper ocean: impact of the eddy diffusivity." Journal of Geophysical Research: Oceans **125**(2): e2019JC015727.

Boufadel, M., T. Ozgokmen, S. Socolofsky, V. Kourafalou, R. Liu and K. Lee (2021). "The transport of the oil following the Deepwater Horizon blowout." Annual Review of Marine Science **(submitted)**.

Canuto, V. and M. Dubovikov (1996). "A dynamical model for turbulence. I. General formalism." Physics of Fluids **8**(2): 571-586.

Charnock, H. (1955). "Wind stress on a water surface." Quarterly Journal of the Royal Meteorological Society **81**(350): 639-640.

Craig, P. D. and M. L. Banner (1994a). "Modeling wave-enhanced turbulence in the ocean surface layer." Journal of Physical Oceanography **24**(12): 2546-2559.

Craig, P. D. and M. L. Banner (1994b). "Modeling wave enhanced turbulence in the ocean surface layer." Journal of Physical Oceanography **24**: 2546-2559.

Cui, F., X. Geng, B. Robinson, T. King, K. Lee and M. C. Boufadel (2020). "Oil Droplet Dispersion under a Deep-Water Plunging Breaker: Experimental Measurement and Numerical Modeling." Journal of Marine Science and Engineering **8**(4): 230.

de Boyer Montégut, C., G. Madec, A. S. Fischer, A. Lazar and D. Iudicone (2004). "Mixed layer depth over the global ocean: An examination of profile data and a profile-based climatology." Journal of Geophysical Research: Oceans **109**(C12).
Delvigne, G. A. and L. J. Hulsen (1994). "Simplified laboratory measurement of oil dispersion coefficient-- application in computations of natural oil dispersion." ENVIRONMENT CANADA, OTTAWA, ON(CANADA). **1**: 173-187.
Delvigne, G. A. and C. Sweeney (1988a). "Natural dispersion of oil." Oil and Chemical Pollution **4**(4): 281-310.
Delvigne, G. A. L. and C. E. Sweeney (1988b). "Natural dispersion of oil." Oil and Chemical Pollution **4**(4): 281-310.
Drennan, W., K. Kahma, E. Terray, M. Donelan and S. Kitaigorodskii (1992). Observations of the enhancement of kinetic energy dissipation beneath breaking wind waves. Breaking waves, Springer**:** 95-101.
Drennan, W. M., M. Donelan, E. Terray and K. Katsaros (1996). "Oceanic turbulence dissipation measurements in SWADE." Journal of Physical Oceanography **26**(5): 808-815.
Ekman, V. W. (1905). "On the influence of the earth's rotation on ocean-currents."
Fingas, M., B. Fieldhouse and J. Mullin (1994). "Studies of water-in-oil emulsions and techniques to measure emulsion treating agents." ENVIRONMENT CANADA, OTTAWA, ON(CANADA). **1**: 213-244.
French-McCay, D. P. (2004). "Oil spill impact modeling: development and validation." Environmental Toxicology and Chemistry: An International Journal **23**(10): 2441-2456.
G. A. L. Delvigne, a. C. E. S. (1988). "Natural dispersion of oil." Oil and Chemical Pollution(4): 281-310.
Garrett, R. M., I. J. Pickering, C. E. Haith and R. C. Prince (1998). "Photooxidation of crude oils." Environmental science & technology **32**(23): 3719-3723.
Gros, J., C. M. Reddy, R. K. Nelson, S. A. Socolofsky and J. S. Arey (2016). "Simulating gas–liquid– water partitioning and fluid properties of petroleum under pressure: implications for deep–sea blowouts." Environmental science & technology **50**(14): 7397-7408.
Gros, J., S. A. Socolofsky, A. L. Dissanayake, I. Jun, L. Zhao, M. C. Boufadel, C. M. Reddy and J. S. Arey (2017). "Petroleum dynamics in the sea and influence of subsea dispersant injection during Deepwater Horizon." Proceedings of the National Academy of Sciences **114**(38): 10065-10070.
Halpern, D. (1976). Structure of a coastal upwelling event observed off Oregon during July 1973. Deep Sea Research and Oceanographic Abstracts, Elsevier.
Johansen, Ø., M. Reed and N. R. Bodsberg (2015). "Natural dispersion revisited." Marine Pollution Bulletin **93**(1): 20-26.
Kara, A. B., P. A. Rochford and H. E. Hurlburt (2000). "An optimal definition for ocean mixed layer depth." Journal of Geophysical Research: Oceans **105**(C7): 16803-16821.
Kitaigorodskii, S. A., M. A. Donelan, J. L. Lumley and E.A.Terray (1983). "Wave turbulence interactions in the upper ocean. Part II: Statistical Characteristics of Wave and Turbulent Components of the Random Velocity Field in the Marine Surface Layer." Journal of Physical Oceanography **13**: 1988-1999.
Large, W. G., J. C. McWilliams and S. C. Doney (1994). "Oceanic vertical mixing: A review and a model with a nonlocal boundary layer parameterization." Reviews of Geophysics **32**(4): 363-403.

Lee, K., M. Boufadel, B. Chen, J. Foght, P. Hodson, S. Swanson and A. Venosa (2015). "Expert panel report on the behaviour and environmental impacts of crude oil released into aqueous environments." Royal Society of Canada, Ottawa, ON.
Lehr, W., R. Jones, M. Evans, D. Simecek-Beatty and R. Overstreet (2002). "Revisions of the ADIOS oil spill model." Environmental Modelling & Software **17**(2): 189-197.
Lehr, W. J. and D. Simecek-Beatty (2000). "The relation of Langmuir circulation processes to the standard oil spill spreading, dispersion, and transport algorithms." Spill Science & Technology Bulletin **6**(3-4): 247-253.
Li, C., J. Miller, J. Wang, S. Koley and J. Katz (2017a). "Size Distribution and Dispersion of Droplets Generated by Impingement of Breaking Waves on Oil Slicks." Journal of Geophysical Research: Oceans **122**(10): 7938-7957.
Li, Z., P. Kepkay, K. Lee, T. King, M. C. Boufadel and A. D. Venosa (2007). "Effects of chemical dispersants and mineral fines on crude oil dispersion in a wave tank under breaking waves." Marine pollution bulletin **54**(7): 983-993.
Li, Z., K. Lee, T. King, M. C. Boufadel and A. D. Venosa (2008). "Assessment of chemical dispersant effectiveness in a wave tank under regular non-breaking and breaking wave conditions." Marine pollution bulletin **56**(5): 903-912.
Li, Z., K. Lee, T. King, M. C. Boufadel and A. D. Venosa (2009a). "Evaluating chemical dispersant efficacy in an experimental wave tank: 2—Significant factors determining in situ oil droplet size distribution." Environmental Engineering Science **26**(9): 1407-1418.
Li, Z., K. Lee, T. King, P. Kepkay, M. C. Boufadel and A. D. Venosa (2009b). "Evaluating chemical dispersant efficacy in an experimental wave tank: 1, dispersant effectiveness as a function of energy dissipation rate." Environmental Engineering Science **26**(6): 1139-1148.
Li, Z., M. L. Spaulding and D. French-McCay (2017b). "An algorithm for modeling entrainment and naturally and chemically dispersed oil droplet size distribution under surface breaking wave conditions." Marine pollution bulletin **119**(1): 145-152.
Mackay, D., I. Buist, R. Mascaraenhas and S. Paterson (1980). Oil spill processes and models. Ottawa, Ontario, Canada, Envrionment Protection Service, Canada. **EE8**.
Mackay, D., A. Chau and Y. C. Poon (1986). A study of the mechanism of chemical dispersion of oil spills. Ottawa, Environmental Protection Agency**:** 150.
Mackay, D., J. Nadeau and C. Ng (1978). A small-scale laboratory dispersant effectiveness test. Chemical Dispersants for the Control of oil spills, ASTM International.
Mackay, D. and W. Zagorski (1982). Studies of water-in-oil emulsions, Environment Canada. Environmental Protection Service. Environmental Impact Control Directorate. Environmental Emergency Branch. Research And Development Division.
Mellor, G. L. and T. Yamada (1982). "Development of a turbulence closure model for geophysical fluid problems." Reviews of Geophysics **20**(4): 851-875.
Naumann, Z. and L. Schiller (1935). "A drag coefficient correlation." Z. Ver. Deutsch. Ing **77**(318): e323.
NRC (2003). Oil in the sea III: inputs, fates, and effects, National Academies Press.
Okuda, K., S. Kawai and Y. Toba (1977). "Measurement of skin friction distribution along the surface of wind waves." Journal of the Oceanographical Society of Japan **33**(4): 190-198.
Pollard, R. T. and R. Millard Jr (1970). Comparison between observed and simulated wind-generated inertial oscillations. Deep Sea Research and Oceanographic Abstracts, Elsevier.

Pope, S. B. (2000). Turbulent Flows, Cambridge University Press.
Prandtl, L. (1953). "Essentials of fluid dynamics: with applications to hydraulics, aeronautics, meteorology and other subjets."
Prince, R. C., K. M. McFarlin, J. D. Butler, E. J. Febbo, F. C. Wang and T. J. Nedwed (2013). "The primary biodegradation of dispersed crude oil in the sea." Chemosphere **90**(2): 521-526.
Reed, M., O. Johansen, F. Leirvik and B. Brørs (2009). "Numerical algorithm to compute the effects of breakingwaves on surface oil spilled at sea." Final Report Submitted to the Coastal Response Research Center. Report F **10968**: 131.
Socolofsky, S. A., J. Gros, E. North, M. C. Boufadel, T. F. Parkerton and E. E. Adams (2019). "The treatment of biodegradation in models of sub-surface oil spills: A review and sensitivity study." Marine Pollution Bulletin **143**: 204-219.
Stevens, C., L. J. Thibodeaux, E. B. Overton, K. T. Valsaraj and N. D. Walker (2017). "Dissolution and Heavy Residue Sinking of Subsurface Oil Droplets: Binary Component Mixture Dissolution Theory and Model-Oil Experiments." Journal of Environmental Engineering **143**(10): 04017067.
Stiver, W. and D. Mackay (1984). "Evaporation rate of spills of hydrocarbons and petroleum mixtures." Environmental science & technology **18**(11): 834-840.
Taylor, G. I. (1953). "Dispersion of soluble matter in solvent flowing slowly through a tube." Proceedings of the Royal Society of London. Series A. Mathematical and Physical Sciences **219**(1137): 186-203.
Taylor, G. I. (1954). "The dispersion of matter in turbulent flow through a pipe." Proceedings of the Royal Society of London. Series A. Mathematical and Physical Sciences **223**(1155): 446-468.
Tennekes, H. L., John L. (1972). A First Course in Turbulence, The MIT Press.
Terray, E. A., M. Donelan, Y. Agrawal, W. M. Drennan, K. Kahma, A. J. Williams, P. Hwang and S. Kitaigorodskii (1996). "Estimates of kinetic energy dissipation under breaking waves." Journal of Physical Oceanography **26**(5): 792-807.
Thorpe, S., P. Bowyer and D. Woolf (1992). "Some factors affecting the size distributions of oceanic bubbles." Journal of physical oceanography **22**(4): 382-389.
Tkalich, P. and E. S. Chan (2002). "Vertical mixing of oil droplets by breaking waves." Marine Pollution Bulletin **44**(11): 1219-1229.
Van Genuchten, M. T. (1982). Analytical solutions of the one-dimensional convective-dispersive solute transport equation, US Department of Agriculture, Agricultural Research Service.
Vlahos, P. and E. C. Monahan (2020). "Recent Advances in the Study of Oceanic Whitecaps: Twixt Wind and Waves."
Ward, C. P. and E. B. Overton (2020). "How the 2010 Deepwater Horizon spill reshaped our understanding of crude oil photochemical weathering at sea: a past, present, and future perspective." Environmental Science: Processes & Impacts **22**(5): 1125-1138.
Zhao, L., M. C. Boufadel, K. Lee, T. King, N. Loney and X. Geng (2016). "Evolution of bubble side Distribution from gas blowout in shallow water." Journal of Geophysical Research: Oceans **121**: doi:10.1002/2015JC011403.
Zhao, L., J. Torlapati, M. C. Boufadel, T. King, B. Robinson and K. Lee (2014a). "VDROP: A comprehensive model for droplet formation of oils and gases in liquids-Incorporation of the interfacial tension and droplet viscosity." Chemical Engineering Journal **253**: 93-106.

Zhao, L., J. Torlapati, M. C. Boufadel, T. King, B. Robinson and K. Lee (2014b). "VDROP: A comprehensive model for droplet formation of oils and gases in liquids-Incorporation of the interfacial tension and droplet viscosity." Chem. Eng. J. **253**: 93-106.

Table 1. General simulation setup

Wind speed	MLD	Roughness height z_0	Initial releasing depth z_{ini}	Depth interval Δz
6 m/s	10 m	0.1 m	10 mm	1 mm
Epsilon	Eddy diffusivity	Total simulation time T	Time interval for transport	Time interval for VDROP
0.1 watt/kg	KPP	8 s	0.01 s	0.001 s
Kb for VDROP	Water density	Water viscosity	Oil-water interfacial tension	Oil density
1	1028 kg/m^3	1.08 cP	13.9 mN/m	887 kg/m^3

Table 2. Simulation setup for different oil slick thickness and viscosity. Bin size increment is 50 microns.

Case number	Oil viscosity	Oil slick thickness	Number of size bins	Initial droplet size	Initial number concentration
1	22.2 cP	0.1 mm	80	4 mm	2.98×10^5 #/m^3
2	22.2 cP	1 mm	180	9 mm	2.62×10^5 #/m^3
3	88.7 cP	0.1 mm	130	6.5 mm	6.95×10^4 #/m^3
4	88.7 cP	1 mm	280	14 mm	6.96×10^4 #/m^3

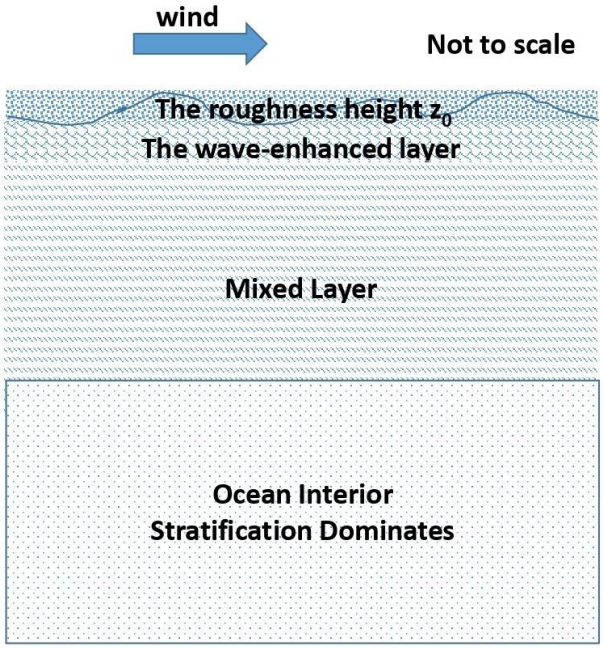

Fig. 1: Schematic of the conceptual approach. The breaker occurs within z_0. Schematic of the roughness height z_0 where the whitecaps occur. The depth z_0 occupies a small fraction of the mixed layer, beneath which, one notes the presence of the ocean interior.

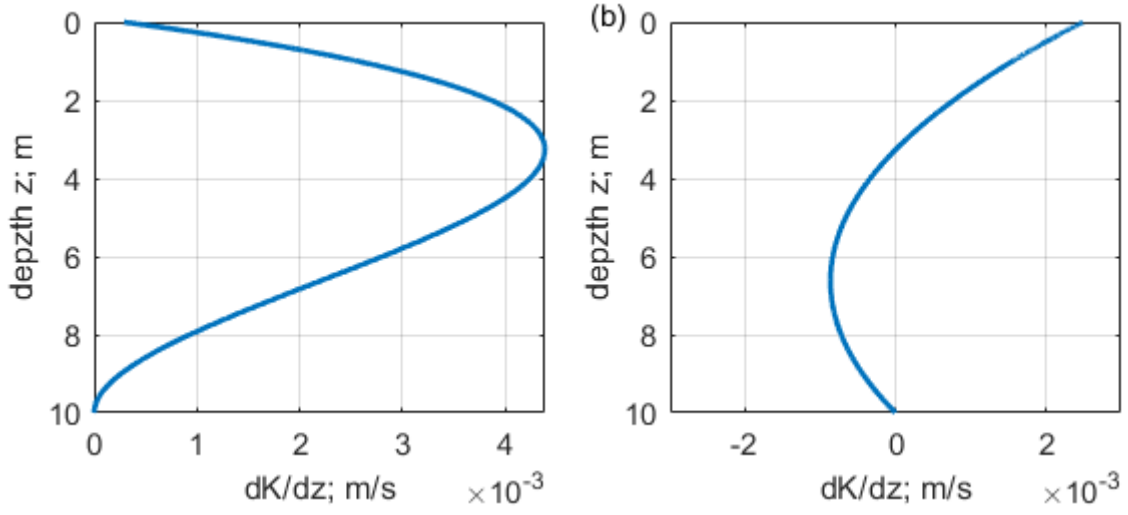

(a) (b)

Fig. 2 (a) The eddy diffusivity profile K as a function of water depth z according to Eq. 2. (b) The gradient of eddy diffusivity dK/dz as a function of water depth z according Eq. 3. Wind speed = 6 m/s; $z_0 = 0.1$ m; MLD = 10 m.

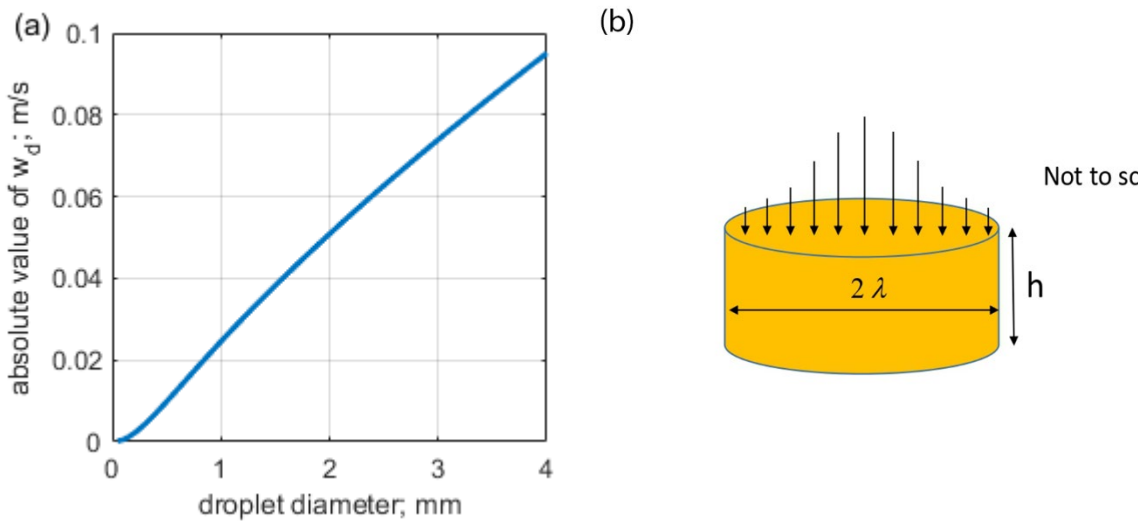

Fig. 3. (a) The terminal rise velocity of droplets due to buoyancy as a function of droplet diameter according to Eq. 8; (b) the schematic of the oil slick. The initial droplet volume is assumed to be the cylinder whose radium is the Taylor microscale of turbulence λ and the height of the oil slick thickness h.

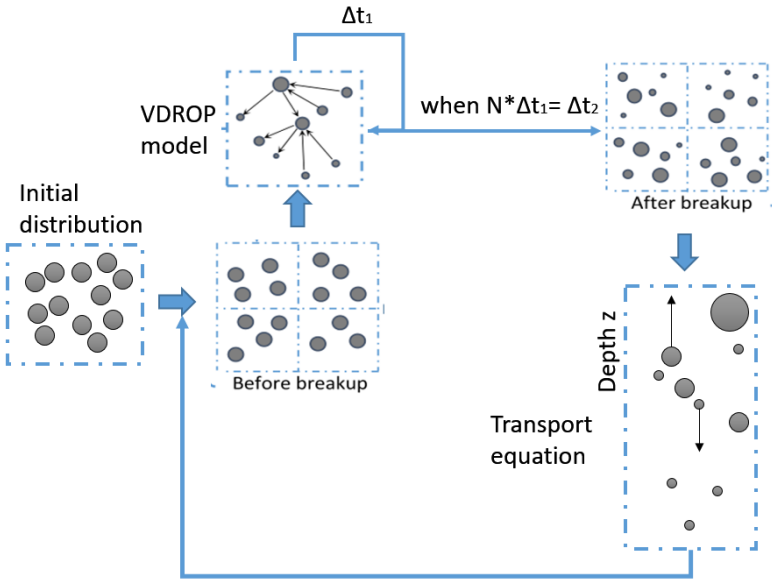

Fig. 4. Schematic illustration of the coupling between the transport equation and the population dynamic model VDROP.

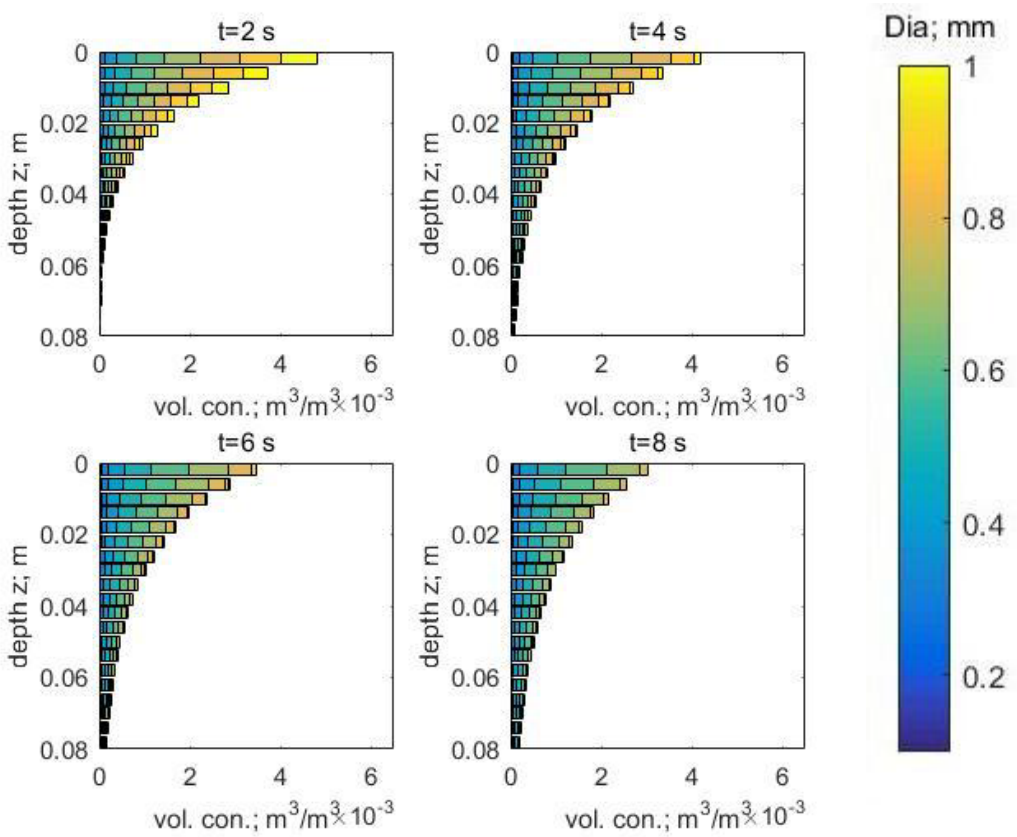

Fig. 5 The volume concentration as a function of depth z at time 2, 4, 6, and 8 s. The different diameter bins are shown as boxes with color indicated by the color bar and the stack of all diameters exhibits the overall performance of droplets with the increase of time. The simulation details are listed in Table 1 and Case 1 in Table 2.

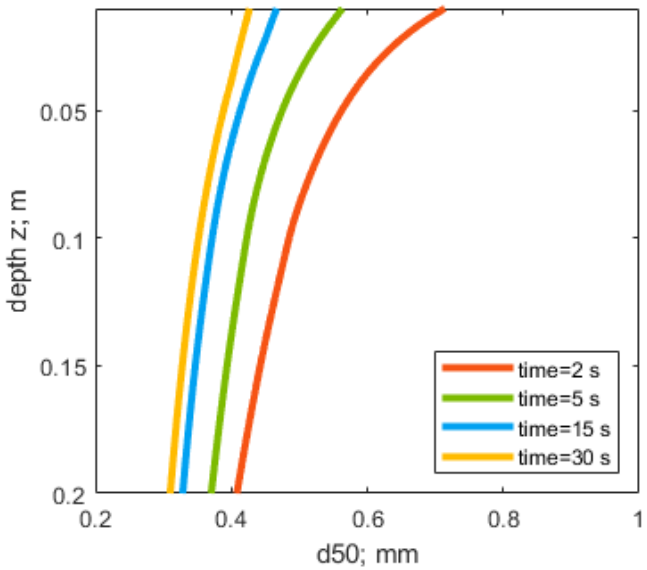

Fig. 6 The volumetric median diameter d_{50} of droplets as a function of depth z for different time t=2, 5, 15, 30 s for Case 1. The d_{50} is the median for the droplet volume within one cell Δz.

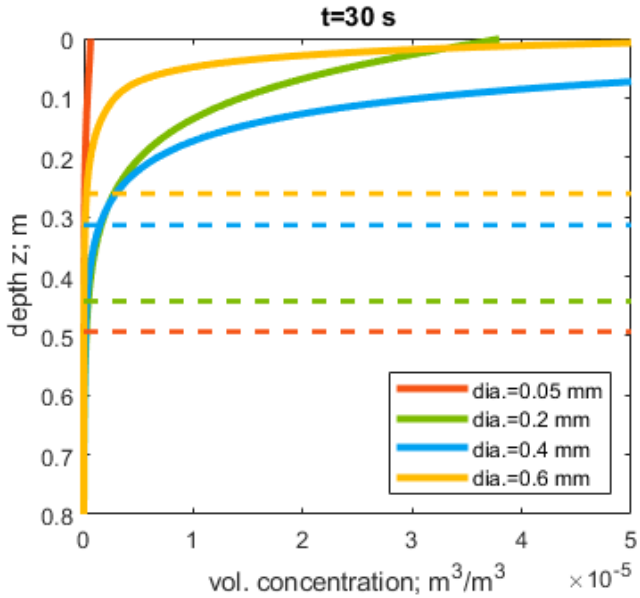

Fig. 7 The volume concentration as a function of depth for droplet diameters of 0.05 mm, 0.2 mm, 0.4 mm and 0.6 mm at t=30 s for Case 1. The dashed line indicates the intrusion depth, which is defined so that the cumulative mass along with the depth reaches 99% of the total current mass for each size bin.

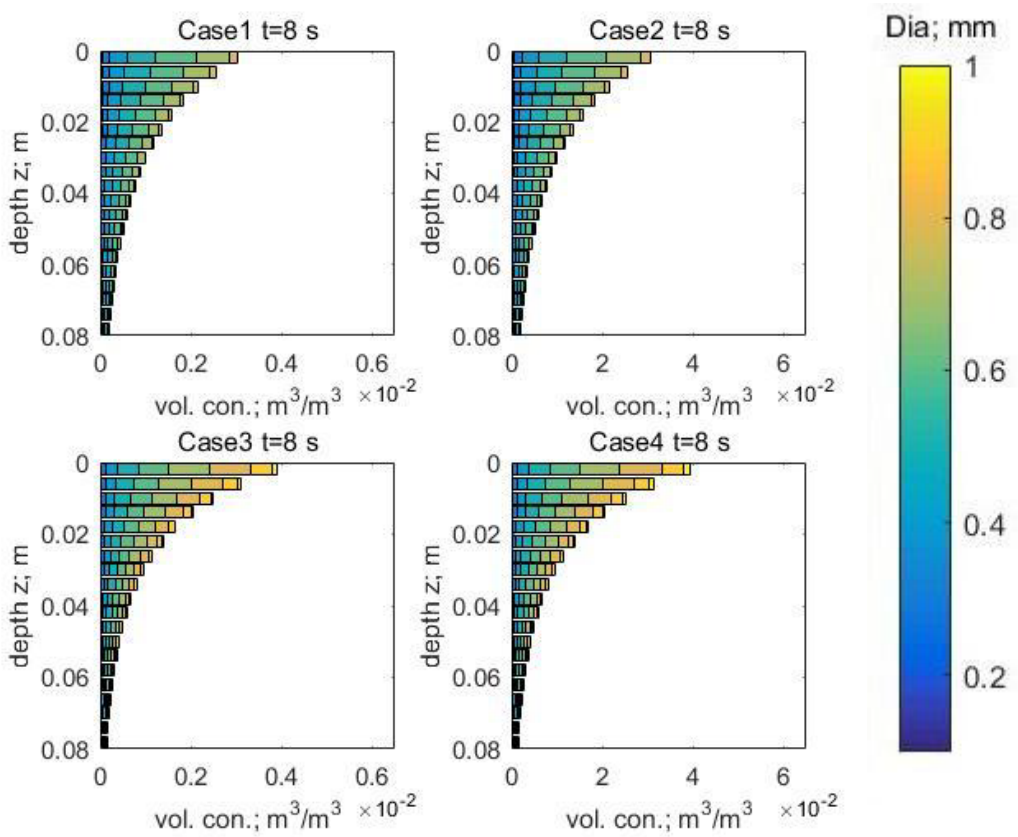

Fig. 8 The volume concentration as a function of depth z at time equals 30 s for four cases listed in Table 2. The different diameter bins are shown as boxes with colors indicated by the color bar and the stack of all diameters exhibits the overall performance of droplets with the increase of time.

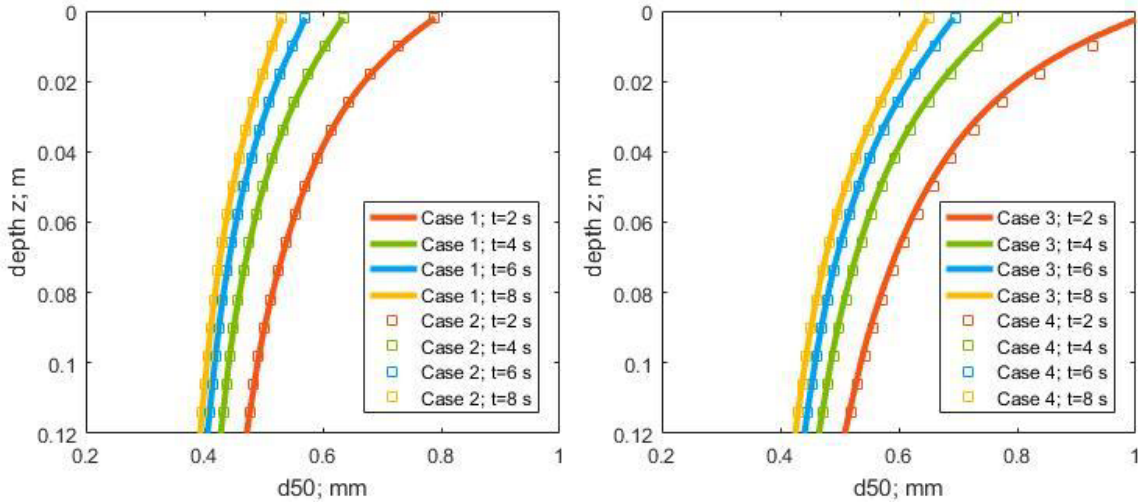

Fig. 9 The volumetric median diameter d_{50} of droplets as a function of depth z for different time t=2, 4, 6, 8 s for four cases listed in Table 2. The left-hand side plot shows the d_{50} for Case 1 and Case 2, where the solid lines represent Case 1 and square symbols represent

Case 2. The right-hand side plot shows the d_{50} for Case 3 and Case 4, where the solid lines represent Case 3 and square symbols represent Case 4.

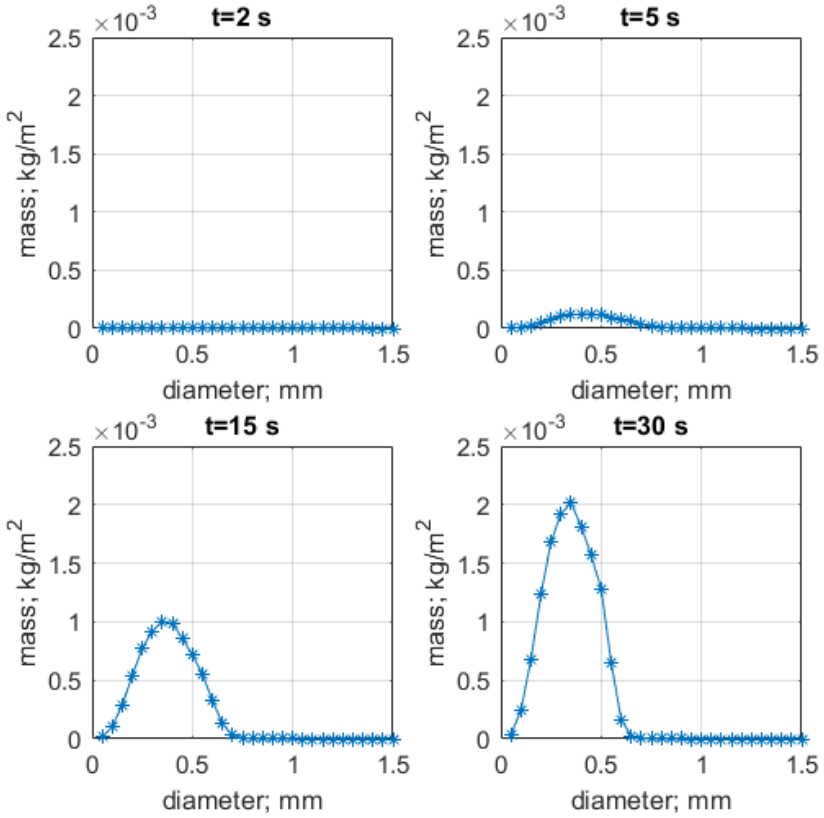

Fig. 10 The entrained mass as a function of droplet size bins at time t=2, 5, 15 and 30 s for Case 1. The entrained mass per unit area (kg/m^2) was computed by summing up the mass of droplets locating below z_b.

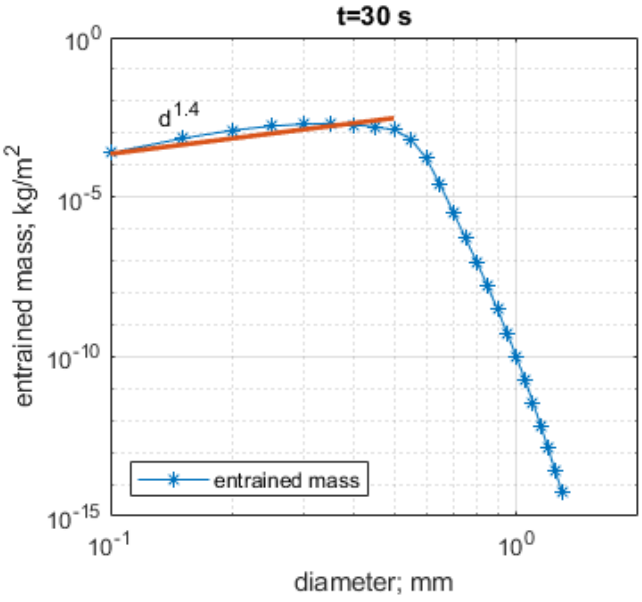

Fig. 11 The entrained mass as a function of droplet size bins at time t=30.0 s. The entrained mass of droplets smaller than 700 μm are fitted to $\sim d^{1.4}$.

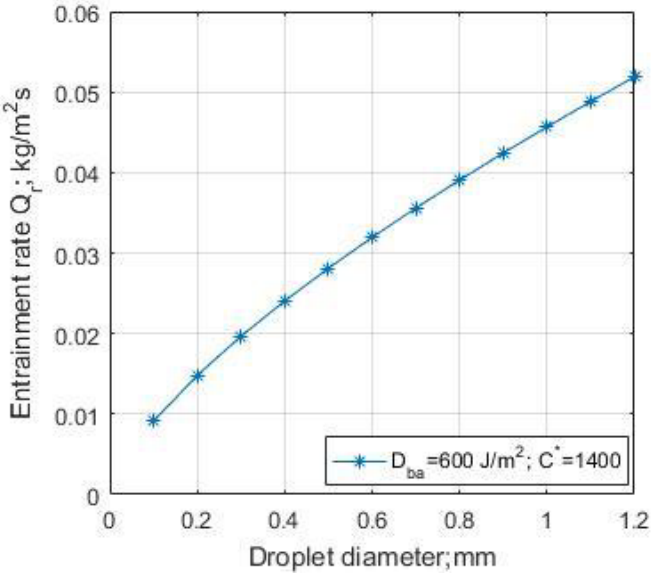

Fig. 12 The entrainment rate Q_r as a function of droplet diameter from Delvigne and Sweeney (1988) based on Eq. 19~20; the dissipated breaking wave energy per unit surface area D_{ba} takes value of 600 J/m^2 and coefficient C^* is adopted as 1400.

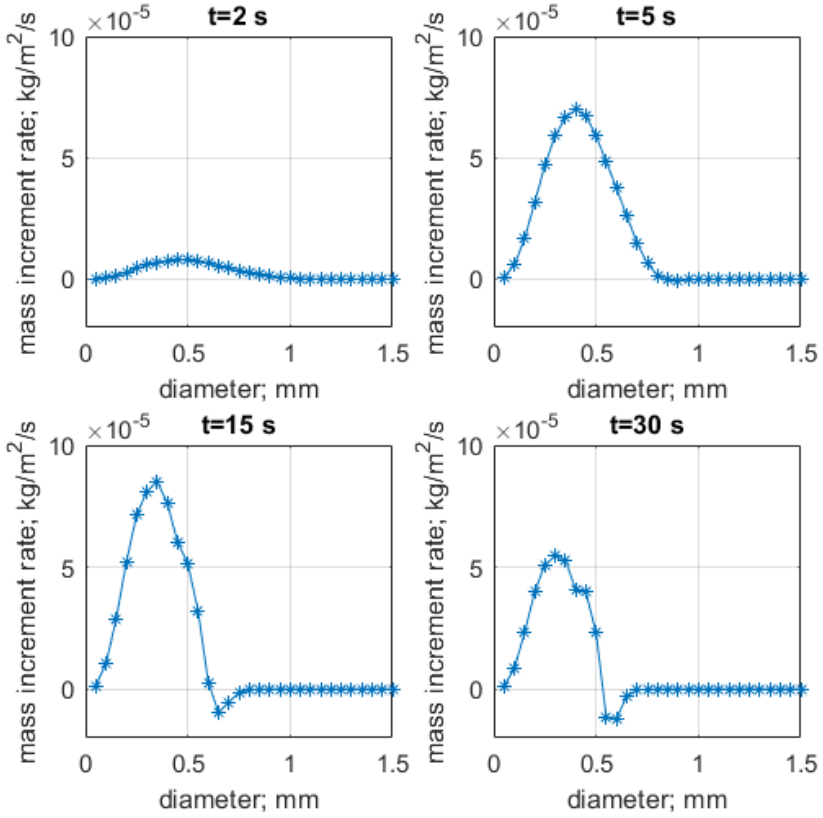

Fig. 13 The entrainment rate Q_r as a function of droplet diameter obtained by the integral model. It is defined as the increment of the entrained droplet mass in every time step and is then divided by the time step.

Reference

Boufadel , M. C., R. Liu, L. Zhao, Y. Lu, T. Ozgokmen, T. Nedwed and K. Lee (2020). "Transport of Oil Droplets in the Upper Ocean: Impact of the Eddy Diffusivity " Journal of Geophysical Research **Accepted**.

Craig, P. D. and M. L. Banner (1994). "Modeling wave-enhanced turbulence in the ocean surface layer." Journal of Physical Oceanography **24**(12): 2546-2559.

Delvigne, G. A. L. and C. E. Sweeney (1988). "Natural dispersion of oil." Oil and Chemical Pollution **4**(4): 281-310.

Large, W. G., J. C. McWilliams and S. C. Doney (1994). "Oceanic vertical mixing: A review and a model with a nonlocal boundary layer parameterization." Reviews of geophysics **32**(4): 363-403.